Measurement of electromigration activation energy in eutectic SnPb and SnAg flip-chip solder joints with Cu and Ni under-bump metallization

Hsiao-Yun Chen and Chih Chen[a)]
Department of Materials Science and Engineering, National Chiao Tung University, Hsin-chu 30010, Taiwan, Republic of China

(Received 27 January 2010; accepted 28 April 2010)

Electromigration activation energy is measured by a built-in sensor that detects the real temperature during current stressing. Activation energy can be accurately determined by calibrating the temperature using the temperature coefficient of resistivity of an Al trace. The activation energies for eutectic SnAg and SnPb solder bumps are measured on Cu under-bump metallization (UBM) as 1.06 and 0.87 eV, respectively. The activation energy mainly depends on the formation of Cu–Sn intermetallic compounds. On the other hand, the activation energy for eutectic SnAg solder bumps with Cu–Ni UBM is measured as 0.84 eV, which is mainly related to void formation in the solder.

I. INTRODUCTION

To meet the demand for high-performance microelectronic devices, miniaturization processes continue to scale down solder-bump pitch and diameter.[1] This has resulted in a dramatic increase in the current density in flip-chip solder bumps. Recently, the electromigration (EM) of flip-chip solder joints has been realized as a serious reliability issue[1,2] because it can lead to failure due to interfacial void formation and large intermetallic compound (IMC) formation inside solder joints.[3–7] Furthermore, because of the combination of the serious current crowding and the Joule heating effect, which cause a nonuniform temperature distribution inside solder joints,[8] it is difficult to predict the failure time of flip-chip solder joints. Choi et al.[9] found that the measured mean time to failure (MTTF) was much smaller at higher current density than the values calculated from Black's equation. They proposed that Black's equation should be modified due to the serious current crowding and the Joule heating effect during current stressing.

According to Choi et al., the MTTF equation can be represented as

$$\mathrm{MTTF} = A\frac{1}{(cj)^n}\exp\left[\frac{Q}{k(T+\Delta T)}\right] \quad , \qquad (1)$$

where MTTF is the current stressing time until failure, A represents a constant that contains a factor involving the cross-sectional area of the joints, j is the current density in amperes per centimeter squared, n is a model parameter for current density, Q is the activation energy, k is Boltzmann's constant, T is the average temperature of the bump, and ΔT is the temperature increase in the solder joint due to the Joule heating effect. The measurement of real temperature is critical in determining the activation energy, since the temperature and activation energy are both located in the exponential term. Several studies have measured activation energy without calibrating the real stressing temperature,[10–12] while others have tried to measure bump temperature by placing a thermocouple or temperature crayon on the surface of a Si die,[10] although these measurements may deviate from the bump temperature. On the other hand, Gee et al. calibrated bump temperature using a special Al trace design to measure the nearest stressing solder bump temperature. Using the temperature coefficient of resistivity (TCR) of the Al trace, their method is able to calibrate temperature more precisely than others. However, they used a daisy-chain structure that cannot monitor the change in the resistance of a single bump; therefore, the failure criteria they used may not be able to detect the first stage of failure in a solder bump.[13]

The definition of electromigration failure can also influence the measurement of activation energy. In general, failure is defined as a 10–20% increase in resistance to Al and Cu interconnects. Most EM studies of solder joints perform electromigration testing using daisy-chain structures that include solder bumps, Al traces in Si dies, and Cu lines on the substrate. Several factors may contribute to an increase in resistance, including void formation, IMC formation, and phase separation in solder bumps. Voids may form in the Al traces on the chip side if daisy-chain structures are used.

Since the cross-sections of Al traces are about two orders of magnitude smaller than those of solder bumps and Cu lines, the resistance of Al trace weights account for over 90% of daisy-chain structure. Furthermore, Al traces have also been reported to suffer electromigration

a)Address all correspondence to this author.
e-mail: chih@faculty.nctu.edu.tw
DOI: 10.1557/JMR.2010.0230

 © 2010 Materials Research Society
CAMBRIDGE JOURNALS
http://journals.cambridge.org Downloaded: 25 Apr 2014 IP address: 140.113.38.11

damage during accelerated EM tests of solder bumps.[14] Therefore, the electromigration damage of Al traces may have a significant influence on the measurement of electromigration failure time and activation energy. Thus, it is necessary to determine a suitable approach to measuring activation energy so that the MTTF of solder joints can be predicted precisely.

This study uses the TCR of Al traces as a temperature sensor to detect the real temperature in solder bumps during current stressing. In addition, Kelvin bump probes were used to monitor the bump resistance during electromigration.[15] A failure criterion was defined as a 20% increase in the bump resistance over its original value. Microstructural analysis was performed to examine the failure mechanism to gain an understanding of the physics behind the activation energy.

II. EXPERIMENTAL

A test layout was designed to measure the resistance of solder bumps and the resistance of their neighboring Al traces, as shown in Fig. 1(a). The solder joints consist of eutectic SnPb and SnAg solder bumps with electroplated 5-μm-thick Cu UBM, as depicted in Fig. 1(b). A 0.3-μm Ti layer was sputtered as an adhesion/diffusion barrier layer between the UBM and the Al trace. Although the SnPb solder is forbidden due to a lead-free policy, it can be used as a comparison to Pb-free solders. The other set of samples consists of eutectic SnAg with 5-μm Cu/3-μm Ni UBMs, as illustrated in Fig. 1(c), referred to in this work as Cu–Ni UBM. The diameter of the solder joint is 130 μm, with a 70-μm-high solder bump and a contact opening with a diameter of 85 μm on the chip side. The metallization on the FR5 substrate consists of 0.05-μm Au and 5-μm electroless Ni. The four bumps were connected by Al traces, and the six nodes were labeled from N1 to N6. Current was applied through nodes N3 and N4, as illustrated in Fig. 1(a). The voltage change of bump B3 can be measured through nodes N5 and N6. In addition, the resistance for the middle segment of the Al trace between B2 and B3 can also be monitored during EM by nodes N1 and N6. To conduct the electromigration test, current stressing was carried out at 135, 150, and 165 °C on a hot plate. A constant current of 0.8 A was passed through the bumps with Cu UBMs, producing a nominal current density of 7.0×10^3 A/cm^2. In contrast, a constant current of 0.9 A was applied through the bumps with Cu/Ni UBMs, producing a nominal current density of 7.9×10^3 A/cm^2 because the electromigration resistance is higher in these bumps.

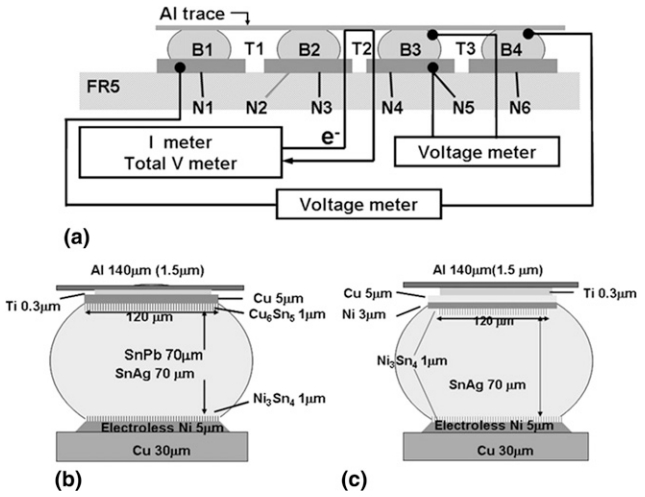

FIG. 1. (a) Cross-sectional schematic of the layout for Kelvin bump probes. The Al trace connected all four solder bumps together. Cross-sectional schematic for the solder bumps with a (b) Cu UBM and (c) Cu/Ni UBM.

The TCR of the middle Al trace was calibrated before the electromigration test to allow it to serve as a temperature sensor. The Al resistance was measured at different temperatures by applying 0.2 A to the Al trace. Infrared (IR) microscopy confirmed that Joule heating was less than 1 °C under this condition. Subsequently, the TCR of the middle Al trace could be obtained. Therefore, the real temperature was detected during an accelerated EM test by simultaneously measuring the resistances of the middle Al trace during detecting the bump resistance in an EM test.

The electromigration failure criterion here is defined as a 20% increase in the original resistance of the bump with downward current stressing. The microstructure of the solder bump was examined by a scanning electron microscope (SEM; JEOL 6500, Tokyo, Japan). A backscattered electron image obtained by SEM was used to examine the morphology of the cross-sectioned SnPb samples and the intermetallic compounds. Furthermore, the compositions of the solder joints and the IMC were analyzed quantitatively by energy dispersive spectroscopy (EDX).

III. RESULTS AND DISCUSSION

Figures 2(a)–2(c) show cross-sectional SEM images of microstructures for the SnAg/Cu, SnPb/Cu, and SnAg/CuNi bumps, respectively, before current stressing. Interfacial IMCs are labeled by the arrows in the figures. Cu–Sn IMCs form in the SnAg and SnPb solder bumps with Cu UBMs on the chip side, whereas Ni_3Sn_4 IMCs occur in the SnAg solder bump with a Ni UBM. The Cu–Sn and Ni–Sn IMCs may be ternary Cu–Ni–Sn IMCs with small amounts of Ni and Cu; this possibility will be discussed later. The electromigration damage generally occurred on the chip side due to serious current crowding in that area. In this study, electromigration failure is defined as the bump resistance increasing by 20%. This definition ensures that the measured electromigration failure time is only related to electromigration damage

http://journals.cambridge.org Downloaded: 25 Apr 2014 IP address: 140.113.38.11

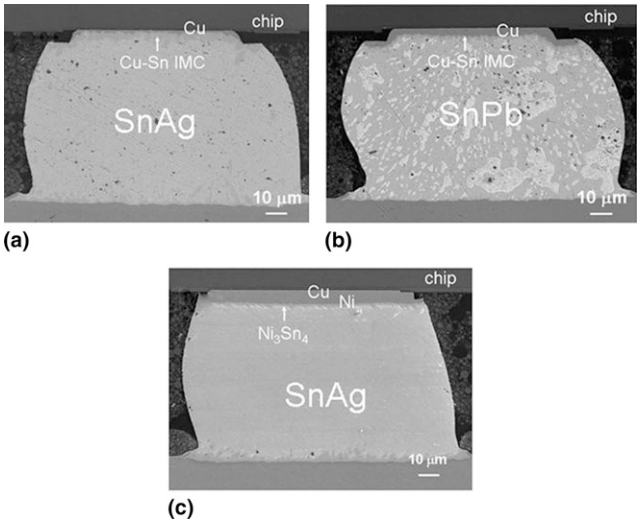

FIG. 2. Backscattered SEM images for solder bumps before current stressing. (a) SnAg bump with a Cu UBM, (b) SnPb bump with a Cu UBM, and (c) SnAg bump with Cu–Ni UBM.

TABLE I. Calibrated temperature and the average failure time of SnAg/Cu, SnPb/Cu, and SnAg/CuNi solder bumps under three testing hot plate temperatures.

	Hot plate temperature (°C)	Calibrated temperature (°C)	Temperature increase (°C)	Average failure time (h)
SnAg/Cu	135	157	22	358
(0.8 A)	150	174	24	180
	165	186	21	56
SnPb/Cu	135	150	15	342
(0.8 A)	150	168	18	144
	165	180	15	83
SnAg/CuNi	135	156	21	431
(0.9 A)	150	170	20	173
	165	184	19	105

in the solder bump, excluding the occurrence of EM damage in Al traces and Cu lines.

In solder joints with Cu UBMs, tiny voids are formed and the Cu UBM is consumed after electromigration failure. Table I lists the average failure time for the SnAg and SnPb bumps under three stressing conditions. Figures 3(a)–3(c) represent the cross-sectional SEM image for the failed SnAg/Cu bump with downward electron flow at 135, 150, and 165 °C, respectively. Some of the 5-μm-thick Cu UBM was consumed and transformed into Cu–Sn IMCs at 135 °C, as shown in Fig. 3(a). On the other hand, the Cu layer was almost consumed and formed Cu–Sn IMC at 150 and 165 °C, as illustrated in Figs. 3(b) and 3(c). Some tiny voids formed at the interface of the IMCs and the solder when stressed at 135 and 150 °C, and then the void location switched to the interface between the Al trace and Cu–Sn IMC at 165 °C, as shown in Fig. 3(c). Current crowded into the solder bump from the upper left corner of the bump,

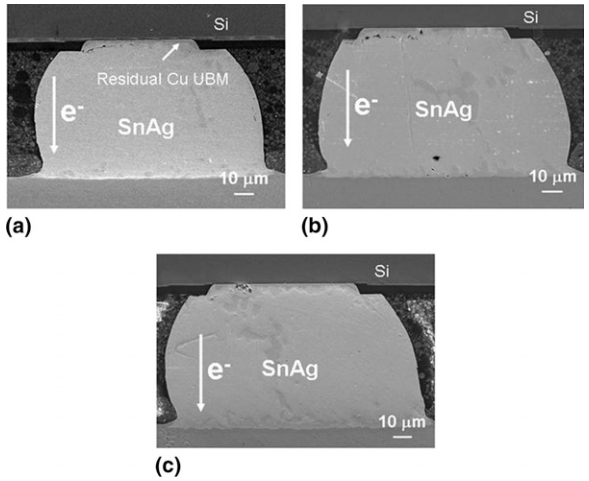

FIG. 3. SEM images of the SnAg bumps with Cu UBMs stressed by a downward current of 0.8 A at (a) 135 °C, (b) 150 °C, and (c) 165 °C. The bump resistance increased by 20% or more.

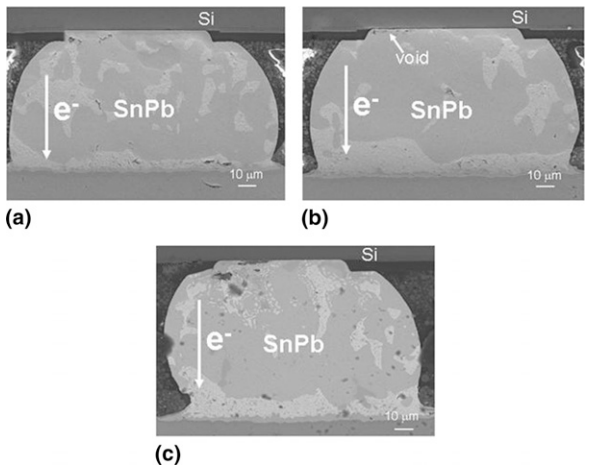

FIG. 4. Backscattered SEM images of SnPb bumps with Cu UBMs subjected to 0.8 A downward current stressing at (a) 135 °C, (b) 150 °C, and (c) 165 °C.

causing the voids to start to form, and higher temperatures also induced rapid dissolution and migration of Cu to the substrate side. Both IMC and void formation contribute to the increase in bump resistance.

For electromigration in the SnPb solder joints, phase segregation also takes place in addition to IMC and void formation. Figures 4(a)–4(c) show the cross-sectional SEM images for bumps stressed at 135, 150, and 165 °C, respectively. Similarly, the bump resistance increased 20% over its original value. The Cu UBM was consumed in the current crowding region on the upper left corner, but there was residual Cu far away from the current crowding/hot spot region. The rate of Cu consumption in SnPb solder appears to be lower than that in the SnAg solder due to the lower solubility of Cu in SnPb solder.[16] In addition, the IMCs migrated to the substrate side. Therefore, tiny voids formed at the interface of the Ti layer and

CAMBRIDGE JOURNALS
http://journals.cambridge.org Downloaded: 25 Apr 2014 IP address: 140.113.38.11

the solder. Phase segregation of Sn-rich and Pb-rich phases in the solder bump might contribute a few percentage points to the increase in resistance.[17] Phase separation is not clear under current stressing at 135 °C, as shown in Fig. 4(a). Pb atoms are the dominant diffusion species when the testing temperature is higher than 150 °C. Therefore, distinct phase separation can be observed in Figs. 4(b) and 4(c) but not in Fig. 4(a). In short, similar to SnAg bumps, IMC and void formation accounts for most of the increase in resistance.

A different failure mechanism was observed in the SnAg/Cu–Ni solder joints during electromigration. Figures 5(a)–5(c) depict the failed bump stressed at 135, 150, and 165 °C, respectively. For the bumps stressed at 135 °C, no obvious consumption of Ni UBM was observed. Instead, voids formed at the interface of the Ni_3Sn_4 and the SnAg solder. At higher stressing temperatures, the consumption of the Cu and Ni UBMs may be occasionally observed, as indicated by one of the arrows in Fig. 5(b). As the stressing temperature increases, the consumption of Cu and Ni UBM becomes more obvious, as presented in Fig. 5(c). However, void formation seems to dominate the electromigration failure in the SnAg/Cu–Ni system.

These results indicate that the Kelvin probes described here are able to detect the early damage of electromigration for various samples and different stressing conditions. In addition, the detected increase in resistance reflects some specific microstructural changes in solder bumps. In the Cu UBM system, the main failure mode is Cu consumption, whereas void formation is the major failure mechanism in the Cu–Ni UBM system.

The central Al trace was adopted as a temperature sensor to measure bump resistance. To ensure that the temperature in the central Al trace was very close to that of the stressed bump, IR microscopy was used to measure the temperature distribution in the Al trace during current stressing. Figure 6(a) shows the temperature distribution in the central Al trace and in the Al pads directly above bumps B2 and B3 stressed at 0.8 A and 100 °C. Because the width was as wide as 100 μm, the local Joule heating effect in the Al trace was not as great as that in the narrower traces.[8] The average temperatures in the five white rectangles were 109.2, 109.9, 109.9, 109.8, and 109.2 °C. Figure 6(b) also shows the Al pad and Al trace temperatures measured using IR versus stressing current. The temperature difference between the Al pad and Al trace increased with stressing current, reaching 1.83 °C at 1.2 A. Under stressing conditions of 0.8 and 0.9 A, the temperature differences are less than 1 °C. Therefore, this method using the central Al trace as a temperature sensor was able to detect bump temperatures during current stressing.

To accurately measure the Joule heating effect, the TCR of the central Al trace was calibrated in an oven. Typically, the TCR can be assumed to be linear and can be simply expressed as

$$R = R_0(1 + \alpha \Delta T) \quad , \tag{2}$$

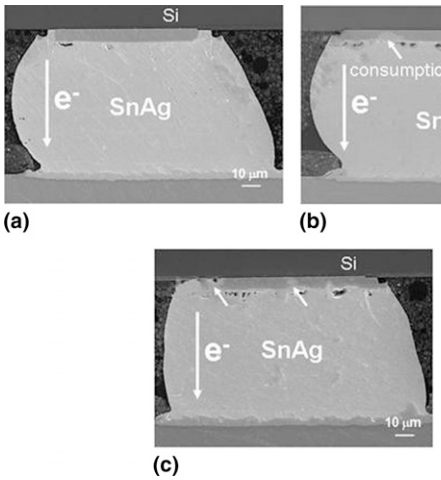

FIG. 5. Cross-sectional SEM images of the failed SnAg bumps with Cu–Ni UBMs subjected to downward current stressing of 0.9 A at (a) 135 °C, (b) 150 °C, and (c) 165 °C.

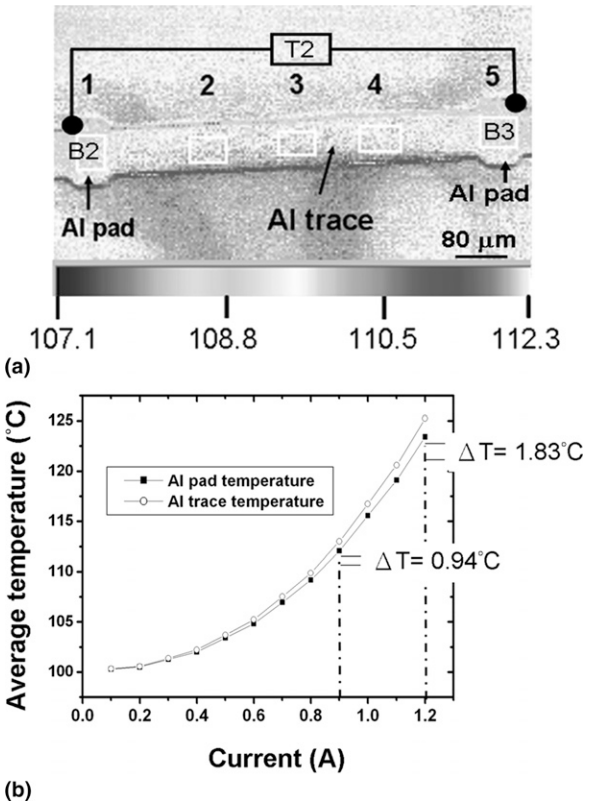

FIG. 6. (a) Temperature distributions in the central Al trace and the Al pad measured by the IR microscope when powered by 0.8 A at 100 °C. Bumps B2 and B3 located directly below the left Al pad and right pad, respectively. (b) The measured Al-pad and Al-trace temperatures under various applied currents.

http://journals.cambridge.org Downloaded: 25 Apr 2014 IP address: 140.113.38.11

where R_0 is the resistance at 50 °C, α is the TCR coefficient, ΔT is the temperature difference, and R is the resistance. To obtain the relationship between the resistance of the Al trace and the temperature of the Al trace, the resistance of the Al trace was measured at various oven temperatures to obtain the TCR coefficient, as shown in Fig. 7. The TCR coefficient of the Al trace was obtained as 4.08×10^{-3} K^{-1} and 4.03×10^{-3} K^{-1} for SnAg and SnPb solders, respectively, with Cu UBM. On the other hand, the TCR coefficient was calculated as 3.95×10^{-3} K^{-1} for SnAg packages with Cu–Ni UBM. These values are very close to the value (3.9×10^{-3} K^{-1}) of bulk Al.

This approach can be used to obtain the real temperature during current stressing. For hot plate temperatures of 135, 150, and 165 °C the real temperatures were measured as 157, 174, and 186 °C, respectively, for the SnAg solders with Cu UBMs; whereas they were 150, 168, and 180 °C for the SnPb solders with Cu UBMs. The temperatures were measured as 156, 170, and 184 °C for the SnAg solders with Cu–Ni UBMs. These data are also reported in Table I. The real temperatures were about 20 and 16 °C higher in the SnAg and SnPb solder bumps, respectively, compared with the hot plate temperatures. The reason for the higher Joule heating effect in SnAg packages is attributed to the thinner Si die. The die thickness of the SnAg and SnPb packages is 250 and 750 μm, respectively. Solder joints with a thinner die have lower heat dissipation ability than those with a thicker die. However, it remains unclear why the calibrated temperature would not increase with increasing hot plate temperature.

To measure the activation energy, at least six samples were stressed in each condition. The average failure time for SnAg solder joints with Cu UBMs was 358, 180, and 56 h at 157, 174, and 186 °C, respectively. Activation energy for electromigration can be obtained using Eq. (1). Figure 8(a) shows the plot of ln(MTTF) against $10^{-3}/T$ with uncalibrated and calibrated temperatures for the SnAg solder. MTTF is adopted as a measure of the average failure time in this study. The activation energy increased from 0.94 to 1.06 eV when the Joule heating effect was considered. Figure 8(b) depicts the results for SnPb solder joints with Cu UBMs. The average failure

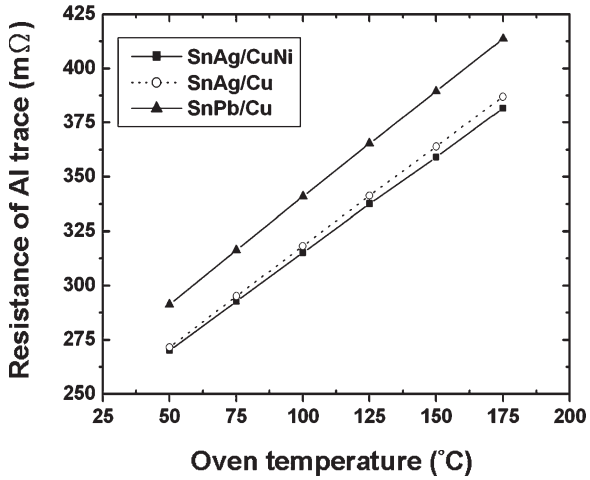

FIG. 7. Plot of the measured resistance of the central Al trace against oven temperature for the three samples. The TCR coefficients can be obtained from the slopes of these curves.

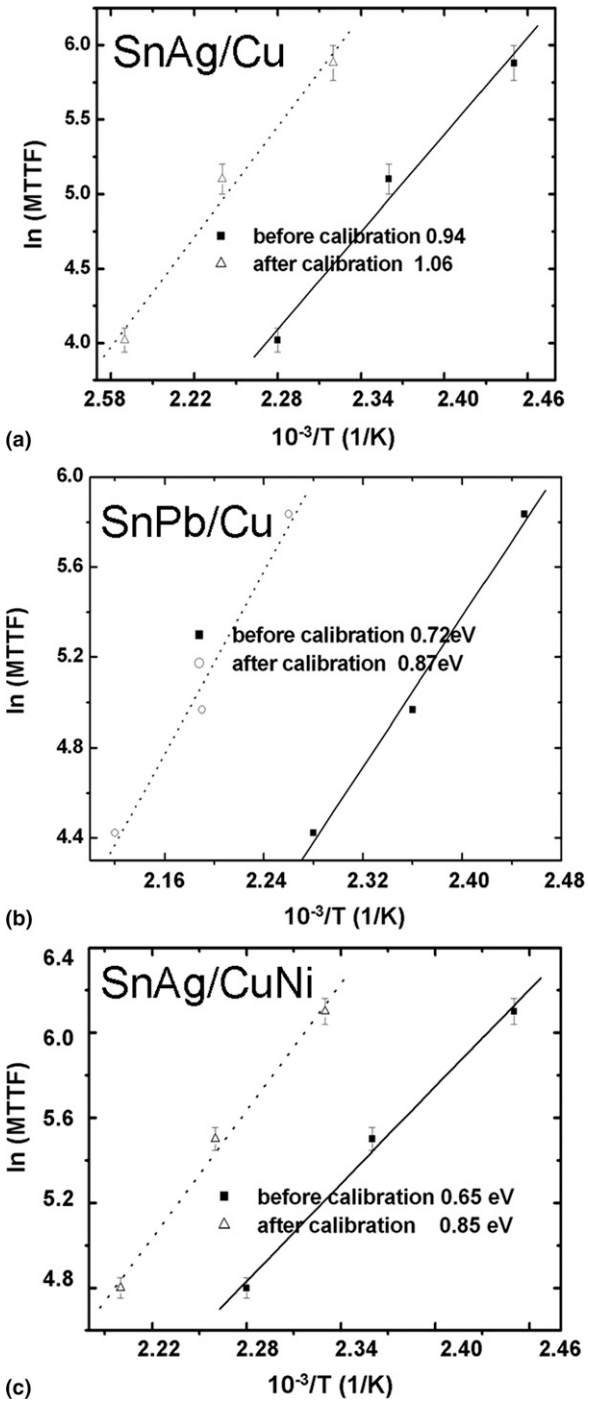

FIG. 8. Plots of MTTF against $10^{-3}/T$ for the (a) eutectic SnAg bumps with Cu UBMs, (b) eutectic SnPb bumps with Cu UBMs, and (c) eutectic SnAg solder with Cu–Ni UBMs.

CAMBRIDGE JOURNALS
http://journals.cambridge.org Downloaded: 25 Apr 2014 IP address: 140.113.38.11

times were 342, 144, and 83 h at 150, 168, and 180 °C, respectively. The measured activation energy changed from 0.72 to 0.87 eV after the temperature calibration, and the difference was as large as 20%. On the other hand, in the SnAg/Cu–Ni system, the average failure times were 431, 173, and 105 h at 156, 170, and 184 °C, respectively. The measured activation energy changed from 0.65 to 0.85 eV after the temperature calibration, as illustrated in Fig. 8(c).

The difference in activation energy may have a significant influence on predicting MTTF in solder joints. For example, for SnPb joints with Cu UBMs at 100 °C, the estimated MTTF ($Ea = 0.87$ eV) was 110 times longer than that when Ea was taken as 0.72 eV from Eq. (1). Therefore, temperature calibration appears to be important in the measurement of activation energy. This approach also makes the physical meaning of activation energy evident. Since Kelvin bump probes were used to monitor the resistance in the solder bumps, the resistance changes solely originated from damage in the solder bump. Resistance changes in the wiring trace and in the contacts can be excluded.

As shown in Figs. 3 and 4, both IMC and void formation contribute to increasing resistance. Thus, the measurement of activation energy mainly involves the processes of Cu–Sn IMC formation and void formation on the chip side. The resistivities for the Cu, SnAg, SnPb, and Cu_6Sn_5 were 1.7, 12.3, 14.6, and 17.5 μΩ-cm, respectively. Therefore, the formation of Cu_6Sn_5 IMCs increases resistance. On the other hand, the voids were tiny and were not discontinuous. It is speculated that these voids do not contribute much to the increase of resistance. Lee et al.[17] studied the solid-state reaction between solders and Cu UBM, reporting that the activation energy for the formation of Cu_6Sn_5 IMC is 1.05 and 0.94 eV for eutectic SnAg and SnPb solders, respectively. These values are very close to the values reported in this study. Therefore, the measured activation energy of electromigration is mainly associated with the formation of Cu_6Sn_5 IMCs.

However, the activation energy we obtained (0.85 eV) in the Cu–Ni UBM system is greater than the formation energy of Ni_3Sn_4 IMCs, which is about 0.17 eV.[18] As shown in Fig. 5, no obvious Ni consumption occurred during the early stage of electromigration. The electromigration was mainly associated with void formation. Therefore, the measured activation energy for eutectic SnAg with Cu–Ni UBMS is much greater than the Ni_3Sn_4 IMC formation energy and is mainly related to void formation.

Note that the IMCs may be $(Cu,Ni)_6Sn_5$ in the SnAg/Cu and SnPb/Cu solder joints because the Ni atoms on the substrate side can rapidly dissolve into the solder and then form $(Cu,Ni)_6Sn_5$ on the chip side. However, the EDX results show that no Ni was detected in the interfacial IMCs on the chip side. For the samples analyzed in Figs. 3–5, the electron wind force pushes the Ni atom back to the substrate side, resulting in a low concentration of Ni in $(Cu,Ni)_6Sn_5$ IMCs on the chip side. The resolution of SEM EDX is approximately 3%. Therefore, no Ni was detected in the interfacial IMCs on the chip sides of the SnAg/Cu or SnPb/Cu solder joints.

On the other hand, both $(Cu,Ni)_6Sn_5$ and $(Ni,Cu)_3Sn_4$ IMCs formed on the chip side in SnAg/Cu–Ni solder joints after current stressing. Figures 9(a) and 9(b) show the compositional analysis of interfacial IMCs near the chip side of the SnAg/Cu–Ni joints after 0.9 A current stressing. Figures 9(a) and 9(b) are enlarged SEM images taken near the chip side for the joints in Figs. 5(b) and 5(c), respectively. The IMCs at Spectra 1 and 7 in Fig. 9 were identified as $(Cu,Ni)_6Sn_5$. The IMC composition is $(Cu_{0.8}, Ni_{0.2})_6Sn_5$ and $(Cu_{0.99}, Ni_{0.01})_6Sn_5$ for Spectrum 1 and 6, respectively.

When the 3-μm-thick Ni layer was consumed locally, Sn may have diffused upward to react with Cu to form

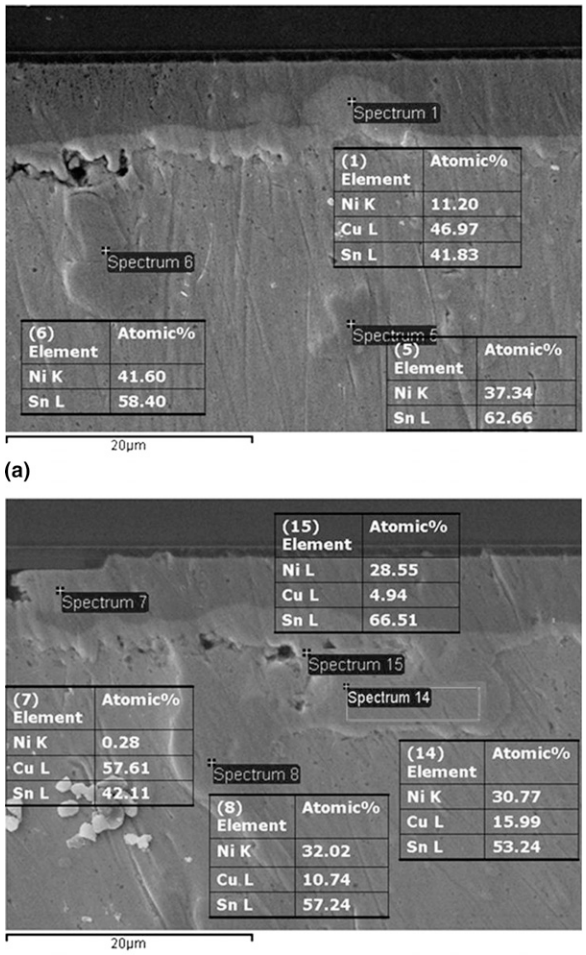

FIG. 9. Compositional analysis of interfacial IMCs near the chip side of the SnAg joints after 0.9 A current stressing at (a) 150 °C [same as the joint in Fig. 5(b)] and (b) at 165 °C [same as the joint in Fig. 5(c)].

http://journals.cambridge.org Downloaded: 25 Apr 2014 IP address: 140.113.38.11

$(Cu,Ni)_6Sn_5$ at those spots. The IMCs at Spectra 5 and 6 in Fig. 9(a) were analyzed as Ni_3Sn_4. It is in the initial stage of EM failure that most of the Ni UBM was not damaged, and thus only a few Cu atoms migrated downward into the solder. We speculate that there are still some Cu atoms in the Ni_3Sn_4 IMC, but their concentration is too low to be detected by SEM EDX. When the stressing temperature was 165 °C, the dissolution of the Cu–Ni UBM increased. Therefore, the Ni_3Sn_4 IMCs were transformed into $(Ni,Cu)_3Sn_4$, as shown in Fig. 9(b). The IMCs at Spectra 8, 14, and 15 were identified as $(Ni,Cu)_3Sn_4$, with a Cu concentration ranging from 5% to 16%. Their IMC compositions are $(Ni_{0.75},Cu_{0.25})_3Sn_4$, $(Ni_{0.66},Cu_{0.34})_3Sn_4$, and $(Ni_{0.85},Cu_{0.15})_3Sn_4$.

IV. CONCLUSION

In summary, this study provides an excellent approach to measure the activation of electromigration in flip-chip solder joints. Using Kelvin bump probes, the bump resistance can be measured accurately, and the electromigration failure is defined as a 20% increase in bump resistance. In addition, the Kelvin probes were also used to measure the resistance of the central Al trace. The measured activation energies were 1.06 and 0.87 eV for the SnAg and SnPb bumps with Cu UBMs, respectively. These values were about 20% greater than those measured without calibrating real temperatures in solder bumps and were close to the formation activation energies of Cu–Sn IMCs. The measured activation energy was 0.85 eV for SnAg bumps with Cu–Ni UBMs and the activation energy is mainly related to the void formation in solder.

ACKNOWLEDGMENT

The authors thank the National Science Council of the Republic of China, Taiwan, for their financial support of this research under Contract No. NSC-96-2628-E-009-010-MY3.

REFERENCES

1. *International Technology Roadmap for Semiconductors* (Semiconductor Industry Association, San Jose, CA, 2003).
2. K.N. Tu: Recent advances on electromigration in very-large-scale-integration of interconnects. *J. Appl. Phys.* **94,** 5451 (2003).
3. L. Zhang, S.Q. Ou, J. Huang, K.N. Tu, S. Gee, and L. Nguyen: Effect of current crowding on void propagation at the interface between intermetallic compound and solder in flip-chip solder joints. *Appl. Phys. Lett.* **88,** 012106 (2006).
4. F.Y. Ouyang, K. Chen, K.N. Tu, and Y.S. Lai: Effect of current crowding on whisker growth at the anode in flip chip solder joints. *Appl. Phys. Lett.* **91,** 231919 (2007).
5. T.L. Shao, Y.H. Chen, S.H. Chiu, and C. Chen: Electromigration failure mechanisms for $SnAg_{3.5}$ solder bumps on Ti/Cr–Cu/Cu and Ni(P)/Au metallization pads. *J. Appl. Phys.* **96,** 4518 (2004).
6. S.H. Chiu and C. Chen: Investigation of void nucleation and propagation during electromigration of flip-chip solder joints using x-ray microscopy. *Appl. Phys. Lett.* **89,** 262106 (2006).
7. Y.H. Lin, C.M. Tsai, Y.C. Hu, Y.L. Lin, and C.R. Kao: Electromigration induced failure in flip-chip solder joints. *J. Electron. Mater.* **34,** 27 (2005).
8. S.H. Chiu, T.L. Shao, and C. Chen: Infrared microscopy of hot spots induced by Joule heating in flip-chip SnAg solders joints under accelerated electromigration. *Appl. Phys. Lett.* **88,** 022110 (2006).
9. W.J. Choi, E.C.C. Yeh, and K.N. Tu: Mean-time-to-failure study of flip-chip solder joints on Cu/Ni(V)/Al thin-film under-bump-metallization. *J. Appl. Phys.* **94**(9), 5665 (2003).
10. S.H. Chae, X.F. Zhang, K.H. Lu, H.L. Chao, P.S. Ho, M. Ding, P. Su, T. Uehling, and L.N. Ramanathan: Electromigration lifetime statistics for Pb-free solder joints with Cu and Ni UBM in plastic flip-chip packages, in *Proceedings of the 56th Electronic Components and Technology Conference* (IEEE, Los Alamitos, CA, 2006), p. 650.
11. Y.S. Lai, K.M. Chen, C.L. Kao, C.W. Lee, and Y.T. Chiu: Electromigration of Sn–37Pb and Sn–3Ag–1.5Cu/Sn–3Ag–0.5Cu composite flip-chip solder bumps with Ti/Ni(V)/Cu under bump metallurgy. *Microelectron. Reliab.* **47,** 1273 (2007).
12. J.H. Lee, G.T. Lim, Y.B. Park, S.T. Yang, M.S. Suh, Q.H. Chung, and K.Y. Byun: Electromigration characteristics of flip chip Sn-3.5Ag solder bumps under highly accelerated conditions. *J. Korean Phys. Soc.* **54**(5), 1784 (2008).
13. S. Gee, N. Kelkar, J. Huang, and K.N. Tu: Lead-free and PbSn bump electromigration testing, in *Proceedings of IPACK 2005* (ASME, New York, 2005).
14. Y.W. Chang, S.W. Liang, and C. Chen: Study of void formation due to electromigration in flip-chip solder joints using Kelvin bump probes. *Appl. Phys. Lett.* **89,** 032103 (2006).
15. K. Zeng and K.N. Tu: Six cases of reliability study of Pb-free solder joints in electronic packaging technology. *Mater. Sci. Eng., R* **38,** 55 (2002).
16. C.K. Chou, C.A. Chen, S.W. Liang, and C. Chen: Redistribution of Pb-rich phase during electromigration in eutectic SnPb solder stripes. *J. Appl. Phys.* **99,** 054502 (2006).
17. T.Y. Lee, W.J. Choi, K.N. Tu, J.W. Jang, S.M. Kuo, J.K. Lin, D.R. Frea, K. Zeng, and J.K. Kivilahti: Morphology, kinetics, and thermodynamics of solid-state aging of eutectic SnPb and Pb-free solders (Sn–3.5Ag, Sn–3.8Ag–0.7Cu and Sn–0.7Cu) on Cu. *J. Mater. Res.* **17**(2), 291 (2002).
18. M.O. Alam and Y.C. Chan: Solid-state growth kinetics of Ni_3Sn_4 at the Sn–3.5Ag solder/Ni interface. *J. Appl. Phys.* **98** 123527 (2005).

CAMBRIDGE JOURNALS
http://journals.cambridge.org Downloaded: 25 Apr 2014 IP address: 140.113.38.11